

# Anisotropic blockade using pendular Rydberg butterfly molecules

Matthew T. Eiles,<sup>1,2</sup> Hyunwoo Lee,<sup>1</sup> Jesús Pérez-Ríos,<sup>1</sup> and Chris H. Greene<sup>1,2,3</sup>

<sup>1</sup>*Department of Physics and Astronomy, Purdue University, 47907 West Lafayette, IN, USA*

<sup>2</sup>*Kavli Institute of Theoretical Physics, University of California,  
Santa Barbara, Santa Barbara, California 93106, USA*

<sup>3</sup>*Purdue Quantum Center, Purdue University, West Lafayette, Indiana 47907, USA.*

(Dated: February 27, 2023)

We propose an experiment to demonstrate a novel blockade mechanism caused by long-range anisotropic interactions in an ultracold dipolar gas composed of the recently observed “butterfly” Rydberg molecules. At the blockade radius, the strong intermolecular interaction between two adjacent molecules shifts their molecular states out of resonance with the photoassociation laser, preventing their simultaneous excitation. When the molecules are prepared in a quasi-one-dimensional (Q1D) trap, the interaction’s strength can be tuned via a weak external field. The molecular density thus depends strongly on the angle between the trap axis and the field. The available Rydberg and molecular states provide a wide range of tunability.

Ultracold dipolar gases provide an ideal environment for the study of novel ultracold chemical reactions or quantum chaos in non-linear dynamical systems [1–5], the design of robust quantum information protocols [6–8], and investigations of universality in few- and many-body physics [9–20]. These promising applications hinge on the premise that regimes exist where the dipole-dipole interaction (DDI) is the dominant force in the system. Recent experiments have partially achieved this in three different systems: ultracold polar molecules [21–24], ultracold lanthanide atoms with large magnetic moments [4, 5, 25–28], and Rydberg atoms in external fields [29–31]. These are challenging experiments: large external fields ( $\sim 10^4$  V/cm) are required to align polar dimers [32], and their production in their rovibrational and hyperfine ground state is a titanic experimental effort [21]. On the other hand, the small atomic magnetic moments require the reduction of the atom-atom interaction using Feschbach resonances [33, 34]. The properties of polar dimers and magnetic atoms are rarely tunable. Rydberg atoms suffer from comparatively short lifetimes, and only interact through the isotropic van der Waals interaction unless dipole moments are induced via an external field [35] or a Förster resonance [36].

The recent observation of ultra-long-range “butterfly” Rydberg molecules [37] shatters these prevailing paradigms. The properties of these *homonuclear* molecules are readily tunable, and they possess gigantic permanent electric dipole moments (PEDMs). These properties are the result of their unique bonding mechanism: the Rydberg electron repeatedly scatters off a nearby perturbing atom, creating a novel chemical bond between these two atoms. This Letter explores the dipolar physics of butterfly molecules in a Q1D array of molecules aligned by a weak ( $< 1$  V/cm) external electric field applied at an angle  $\theta$  relative to the longitudinal trap axis. Intermolecular forces prevent the resonant excitation of two molecules within the butterfly blockade radius  $R_b(\theta)$ , where the anisotropic intermolecular

potential,  $V(R_b, \theta)$ , exceeds the laser bandwidth,  $\Omega$  ( $\sim 0.5$  MHz).  $R_b(\theta)$  can be tuned by the applied field: at the “magic angle” satisfying  $P_2(\cos \theta_M) = 0$  ( $P_L$  is the Legendre polynomial of order  $L$ ) the DDI vanishes and higher-order terms in the molecular interaction, namely the quadrupole-quadrupole/dipole-octupole and van der Waals, dominate. Thus, the molecular density reveals these interactions via its dependence on  $\theta$ . This high tunability rendered by our proposal allows for the design of a density regime where the butterfly molecules are immersed in a sea of bosons, which may have important implications in the study of the polaron problem. In particular, it offers an intriguing scenario for the study of polaron interactions in a quantum degenerate gas.

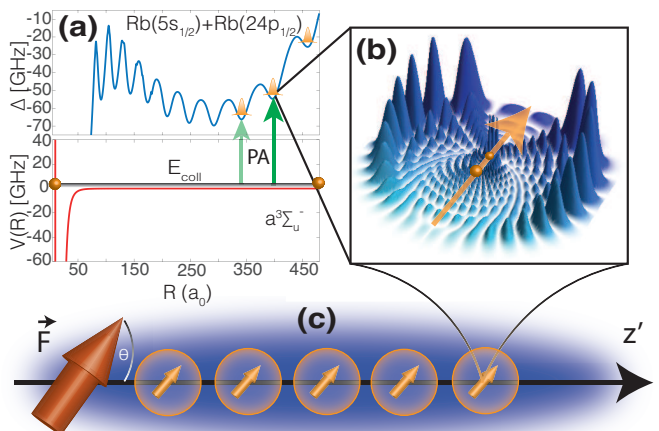


FIG. 1. a) The proposed single-photon photoassociation scheme. The target bound state is selected by the laser frequency. b) The electronic probability density  $\rho|\Psi(\rho, z)|^2$  in cylindrical coordinates. c) The experiment: extremal pendular butterfly molecules in a Q1D cigar-shaped cloud are aligned by the electric field at an angle  $\theta$ . The blockade radius prevents simultaneous excitation of two close molecules.

The organization of this Letter follows the hierarchy of energy scales in this system. First, the properties of butterfly molecules, which are bound by several GHz and have electronic/vibrational spacings of a few GHz are discussed. Next, the pendular states are calculated within the rigid-rotor approximation; their energy splittings are a few tens of MHz. The intermolecular interactions are calculated perturbatively, and their maximum strength for our considerations is restricted by  $\Omega$  ( $\sim 100$ kHz). Once this interaction is calculated the density of molecules is readily obtained as a function of  $\theta$ .

Butterfly molecules consist of a Rydberg atom bound to a ground state atom [38]. The de Broglie wavelength of the electron is much larger than the atom, validating a description of the scattering process in terms of contact pseudopotentials proportional to  $-\tan \delta_L/k^{(2L+1)}$ , where  $\delta_L$  is the elastic phase shift for partial wave  $L$  and  $k$  is the electron's momentum [39, 40]. The contributions from partial waves  $L > 0$  typically vanish at ultracold temperatures. However, the presence of a  $P$ -wave shape resonance causes  $\tan \delta_1$  to diverge, resulting in a potential curve descending from the  $n$  atomic line to below the

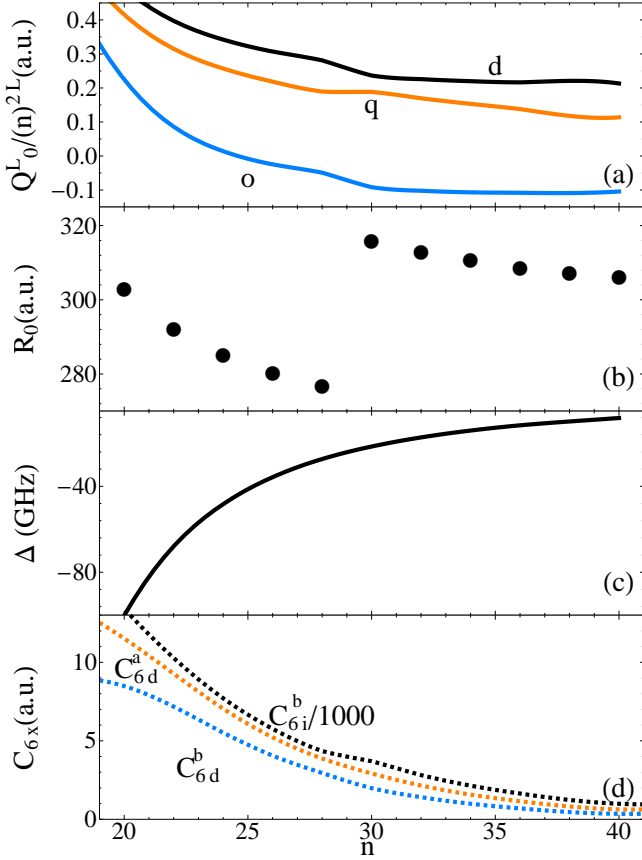


FIG. 2. Properties of the deepest pendular state as a function of  $n$ : a) multipole moments, labeled  $d = Q_0^1/n^2$ ,  $q = Q_0^2/n^4$ , and  $o = Q_0^3/n^6$ ; b) bond lengths; c) binding energies; d) van der Waals coefficients (see Eq. 4).

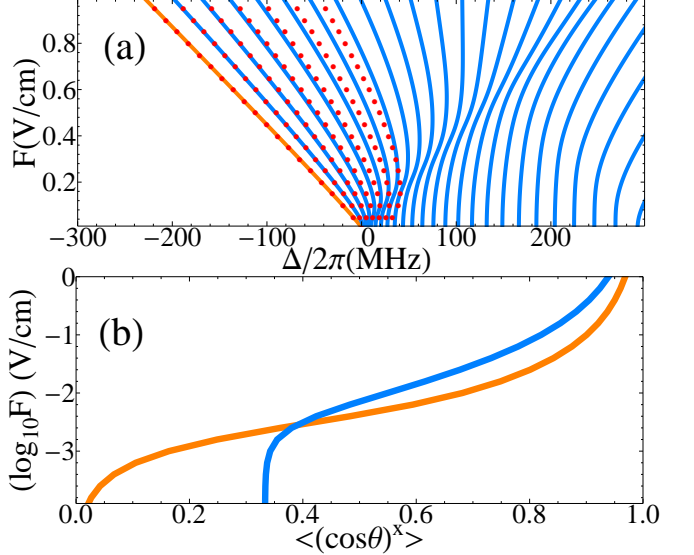


FIG. 3. (a) Stark spectrum of the  $n = 24$  pendular states, showing the energy shift  $\Delta$  as a function of the applied electric field for  $M_N = 0$ . The red points correspond to the two-dimensional harmonic oscillator approximation. (b) Orientation ( $x = 1$ ) (orange) and alignment ( $x = 2$ ) (blue) of the lowest pendular state [orange line in (a)].

$(n+2)p$  Rydberg level [41]. Throughout  $n$  will refer to the principal quantum number of the hydrogenic manifold higher in energy than the  $(n+2)p$  state, which is red-shifted by its quantum defect  $\mu_p \approx 2.65$ . Level repulsion from the  $n-1$  hydrogenic manifold constrains the divergence [41–43]. The potential curve oscillates as a function of the internuclear distance  $R$  and molecules form in the potential wells mirroring the  $p$ -wave wave function [37]; the relatively high  $p$ -character found in the butterfly wave function allows for photoassociation in a dense condensate through a single photon process. Neglecting spin, the pseudopotentials are

$$V(\vec{R}, \vec{r}) = 2\pi a_S \delta(\vec{r} - \vec{R}) + 6\pi a_P \vec{\nabla} \cdot \delta(\vec{r} - \vec{R}) \vec{\nabla}. \quad (1)$$

The generalization of Eq. 1 to include spin-dependent scattering parameters, so that  $a_S \rightarrow a_{1S_0, 3S_1}$ ,  $a_P \rightarrow a_{1P_1, 3P_{0,1,2}}$ , is detailed in [44]. The full Hamiltonian  $H = H_0 + H_{SO} + V + H_{HF}$  includes the Rydberg electron's Hamiltonian,  $H_0$ , the Rydberg spin-orbit interaction  $H_{SO}$ , and the hyperfine splitting of the ground state atom,  $H_{HF}$  [44–46]. Diagonalization of  $H$  reveals binding energies, bond lengths, and multipole moments [44]. A typical potential curve and vibrational states are plotted in Fig. 1a. The electronic state associated with this potential is shown in Fig. 1b and consists of a mixture of Rydberg states that maximizes the radial derivative of the wave function at  $\vec{r} = \vec{R}$ . Fig. 2 displays various molecular parameters of the ground state as a function of  $n$ . Greater tunability is possible if different molecular states are excited.

In the absence of external fields, polar molecules ro-

tate freely with random orientations. Application of a field shifts the molecular energy through the dipole-field coupling  $-\vec{d} \cdot \vec{F}$ , where  $\vec{F}$  is the electric field and  $\vec{d}$  is the molecular PEDM. Setting the quantization axis parallel to the electric field, the molecular Hamiltonian is  $H_{\text{mol}} = B_e \hat{N}^2 - dF \cos \theta$ , with rotational constant  $B_e$  and rotational angular momentum operator  $\hat{N}$  [47]. When the dimensionless parameter  $\omega = \frac{dF}{B_e}$  is large, the rotational states become trapped in a nearly harmonic potential and are called pendular states in analogy with the harmonic oscillator [48, 49]. Owing to their exceptionally large  $\omega \sim 10^2 - 10^3$ , the pendular regime is reached in butterfly molecules with fields  $\sim 1$  V/cm, four orders of magnitude lower than needed for typical heteronuclear molecules [21, 37]. These states are found by diagonalizing  $H_{\text{mol}}$  in the basis of spherical harmonics  $Y_{NM_N}(\theta, \phi)$ ;  $M_N$  is a good quantum number. The pendular states  $|\tilde{N}M_N\rangle$  are characterized by their librational state,  $\tilde{N}$ . The ground state,  $|00\rangle$ , is the most aligned pendular state. Fig. 3a shows the resulting Stark spectrum for the  $n = 24$  case. Fig. 3b shows  $\langle \cos \theta \rangle$  and  $\langle \cos^2 \theta \rangle$ .

Fig. 1c depicts a sketch of the geometry of our proposal. The electric field points in the lab frame's  $z$  axis; a strongly confining potential in the  $x$  and  $y$  dimension creates a Q1D chain of Rb atoms in the  $z'$  direction [50], where  $\cos \theta = \hat{z} \cdot \hat{z}'$ . The laser is tuned to excite the  $|00\rangle$  pendular butterfly state. Two molecules, labeled  $A$  and  $B$  are separated by an inter-molecular distance  $R_{AB}$  that depends on the atomic density and the long-range inter-molecular interaction, given by the two-center multipolar expansion of the Coulomb force [51–55]. In the present case, this takes the form [56]

$$\hat{V} = \sum_{L_A, L_B} q(L_A)q(L_B) \frac{f_{L_A, L_B}^n}{R_{AB}^{L+1}} \sum_{m_A, m_B, m} \binom{L_A \ L_B \ L}{m_A \ m_B \ m} \times D_{m_A 0}^{L_A}(\theta_A, \phi_A)^* D_{m_B 0}^{L_B}(\theta_B, \phi_B)^* D_{m 0}^L(\theta, 0)^*, \quad (2)$$

where  $L = L_A + L_B$  and  $D_{m_X 0}^{L_X}(\theta_X, \phi_X)^*$  is a Wigner D-Matrix rotating the multipole operator between the lab and molecule frame.  $D_{m 0}^L(\theta, 0)$  describes the geometry of the trap axis relative to the electric field axis, and

$$f_{L_A, L_B}^n = (-1)^{L_A} n^{2L} \left[ \frac{(2L+1)!}{(2L_A)!(2L_B)!} \right]^{1/2}. \quad (3)$$

The reduced multipole moment of molecule  $X$  averaged over the vibrational molecular wave function is  $q(L_X) = Q_0^{L_X}/n^{2L_X}$ . These are shown for a range of  $n$  in Fig. 2a. Eq. (2) is valid if  $R_{AB} > 2(\sqrt{\langle r_A^2 \rangle} + \sqrt{\langle r_B^2 \rangle})$  [57]. This criterion is satisfied for all distances here.

The intermolecular interaction is calculated to order  $(R_{AB})^{-6}$ , requiring up to second order in perturbation theory. The zeroth order wave functions are the pendular states obtained by diagonalizing  $H_{\text{mol}}$ , whose energy spacings are typically an order of magnitude smaller than the vibrational or electronic spacings. We neglect

contributions from other electronic or vibrational levels in the second-order sum over intermediate states, which should introduce errors in the  $1/R_{AB}^6$  potentials of 10% or less due to the larger energy separations. The overall  $n$ -scaling of the multipole moments factors out, along with an additional  $n^3$  for the second-order terms from their energy denominators. This gives

$$\begin{aligned} V(R_{AB}, \theta) = & \quad (4) \\ & - \frac{2C_3 d^2 n^4}{R_{AB}^3} P_2(x) - \frac{8n^8}{R_{AB}^5} P_4(x) (C_{5a} d o - C_{5b} q^2) \\ & - 2 \frac{4d^4 n^{11}}{R_{AB}^6} \left( C_{6i}^a [P_2(x)]^2 + C_{6i}^b \frac{(xy)^2}{4} \right) \\ & - \frac{4d^4 n^{11}}{R_{AB}^6} \left( C_{6d}^a [P_2(x)]^2 + \frac{C_{6d}^c}{4} y^4 + C_{6d}^b \frac{(xy)^2}{4} \right), \end{aligned}$$

where  $x = \cos \theta$ ,  $y = \sin \theta$ , and  $C_q > 0$ . We obtain  $C_3 \sim 0.95$ ,  $C_{5a} \sim 0.83$ , and  $C_{5b} \sim 0.63$  for the first-order coefficients, independent of  $n$  within 2% over the range  $n = 20 - 40$ . The second-order coefficients vary slowly with  $n$  as seen in Fig. 2d. These van der Waals terms have been split into induction ( $C_{6i}$ ) and dispersion ( $C_{6d}$ ) terms, where induction corresponds to the dipole-induced-dipole force; in the sum over virtual states, the induction term is restricted to include only virtual states with a single molecule in the excited state, while both are excited in the dispersion term.

The coefficients in Eq. 4 are determined by the matrix elements  $K_{\tilde{N}M_N, LM}^{\tilde{N}'M'_N} = \langle \tilde{N}M_N | Y_{LM}(\theta, \phi) | \tilde{N}'M'_N \rangle$ , which vanish if  $M + M'_N - M_N \neq 0$ . As a result the first order terms depend on  $\cos \theta$  alone, while to second-order the DDI can couple also to  $|M_N| = 1$  virtual states, introducing  $\sin \theta$ . Several unexpected properties of these coefficients emerge: the independence of the first-order coefficients on  $n$ , the numerical relationship  $\frac{C_{6i}^a}{2} = \frac{C_{6d}^c}{9} = C_{6d}^a$ , and the large relative size of  $C_{6i}^b$  ( $\sim 1000$  times larger than the others). In the large  $\omega$  limit  $H_{\text{mol}}$  reduces to the two-dimensional harmonic oscillator Schrödinger equation in polar coordinates [58, 59], which elucidates these properties. The harmonic oscillator wave functions  $\Psi_{\tilde{N}M_N}(\xi, \phi)$  and energies  $E/B_e = \sqrt{2\omega}(2\tilde{N} + |M_N| + 1) - \omega$  are readily obtained and excellently describe states deep in the pendular regime [60]. Using these as zeroth order states confirms the earlier results to within 10% using only states with  $\tilde{N} \leq 1$  and  $|M| \leq 1$  to reach convergence. The properties of the coefficients are largely determined by the analytical asymptotic forms of the four matrix elements that appear in this calculation:  $K_{00,10}^{10} \sim a\omega^{-1/2}$ ,  $K_{00,1-1}^{01} \sim a(\omega/2)^{-1/4}$ ,  $K_{00,1-1}^{11} \sim a(2\omega)^{-3/4}$ , and  $K_{00,10}^{00} \sim a(2^{1/2} - \omega^{-1/2})$  as  $\omega \rightarrow \infty$  ( $a = \sqrt{3/8\pi}$ ). The  $K_{00,L0}^{00}$  terms alone contribute to the first-order coefficients, and at large  $\omega$  they become constant. The  $K_{00,1-1}^{01}$  term dominates the others as  $\omega \rightarrow \infty$ , determining, along with the geometric

factors associated with the spherical harmonics and the Wigner 3-J symbol, the properties of the second-order coefficients. At large  $\omega$ , the results  $\frac{C_{6i}^a}{2} = \frac{C_{6d}^c}{9} = C_{6d}^a$  are reached asymptotically [61]. This dominant term also determines the ratio  $C_{6i}^b/C \sim \sqrt{\omega}$ , where  $C$  is any other second-order coefficient [62].

Fig. 4 displays the key result of this Letter. Panel a shows the predicted density of butterfly molecules for a laser bandwidth  $\Omega = 0.5\text{MHz}$  for several  $n$  values. The  $n$ -dependent magic angle  $\theta_{M,n}$  ranges from  $56.7^\circ - 57.3^\circ$  (0.99-1.0 radians) [63] and differs slightly from the DDI magic angle  $\theta_M = 54.7^\circ$  due to the higher-order  $n$ -dependent terms in  $V(R_{AB}, \theta)$ . Decreasing with  $n$  due to the stronger interactions at higher  $n$ , the density is  $\sim 4$  times greater at  $\theta_{M,n}$  than at  $\theta = 0$  and corresponds to a maximum blockade radius of  $\sim 1\mu\text{m}$ . The  $\theta$ -dependence in Panel a is rescaled to exaggerate the behavior near  $\theta_{M,n}$ , and emphasizes the discontinuity just above  $\theta_{M,n}$  (discussed below). Panel b displays a density plot of the potential surface for  $n = 24$ , where blue(red) colors parallel to the x(y) axis represent the attractive(repulsive) potential. Lines of force are superimposed, and the inner(outer) white contours represent the blockade radius for  $0.5(0.1)\text{MHz}$ . In the bottom panel simulated ion yields are displayed for several paradigmatic angles, showing the slow increase in created molecules as  $\theta$  increases followed by a sudden rise in number at  $\theta = \theta_{M,n}$ . A striking behavior is seen for  $\theta$  just greater than  $\theta_{M,n}$ : the density drops discontinuously. This stems from the interplay between the attractive van der Waals interactions and the DDI. When the latter interaction is repulsive, a potential barrier is created for  $R_{AB}$  greater than the inner crossing point where  $V(R_{AB}, \theta) = -\Omega$ . As the DDI increases relative to the van der Waals terms this repulsive barrier increases until it reaches  $+\Omega$ , shifting the blockade radius suddenly. Fig. 4 reveals the proposed experimental signature of these long-range interactions, and an ion-imaging experiment [35] can witness the anisotropy of these interactions through the dramatic change in density near  $\theta_{M,n}$ .

The required atomic densities are large: a density of  $2 \times 10^{15}\text{cm}^{-3}$  gives two butterfly molecules per blockade volume. More favorable conditions are granted at higher Rydberg levels, where the interaction strengths are greater and the formation probability is enhanced due to the larger internuclear distance. A narrower bandwidth laser extends the effective range of the intermolecular interactions. Finally, an alternative setup could use a Q1D optical lattice in a doubly-occupied Mott insulator state [64].

This experimental realization is not restricted to Rb butterfly molecules. Another scheme involves the excitation of long-range “trilobite” molecules through two-photon excitation of  $\text{Cs}_2$  [65, 66]. Bound by the s-wave scattering potential of Eq. 1, these molecules have larger bond lengths and dipole moments than butterfly

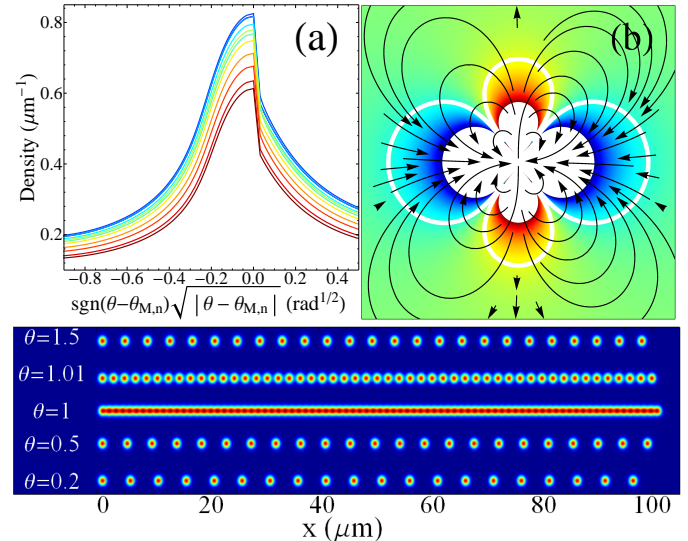


FIG. 4. a) Simulated density as a function of the angle between the field and trap axes. As  $n$  increases from 20-40 the color changes from blue to red. b) The interaction potential  $V(R_{AB}, \theta)$  is shown in cartesian coordinates for  $n = 24$ , where blue(red) regions are attractive(repulsive). The inner white region (outer white contour) is the blockade radius satisfying  $|V(R_B)| \geq \Omega$ , where  $\Omega = 0.5(0.1)\text{MHz}$ . Lines of force are overlaid. The length of a side of the figure is  $2 \times 10^5$  a.u. Bottom) Simulated ion measurements for a 100 micron trap for five different angles and for  $n = 24$ .

molecules, allowing for more favorable density conditions and stronger alignment. However, their lifetimes are typically shorter by a factor of two or more, the two-photon process required to access the  $(n-4)S$  character of the trilobite admixture necessitates a higher intensity laser source, and their tunability is limited since they are typically bound in just the outermost potential well. Another trilobite excitation scheme has been proposed in Ca, where trilobite-like molecules can be excited via two-photon excitation of the  $nD$  state, which is admixed into the degenerate manifold by perturbations from doubly excited states [67]. Even low- $l$  molecules exhibit weakly polar behavior from their small admixture of trilobite-sized dipole moments [68, 69].

Our proposal presents an effective method to control the density of pendular butterfly molecules in a Q1D trap using a weak static electric field. As a consequence of the inherently mixed nature of this scenario it can be viewed as a system of dipolar impurities immersed in a sea of bosons, and thus it can be exploited to study polaron-polaron interactions in ultracold gases. The tunability of the polaron interaction provides information about the role of the internal structure of the impurities in the dynamics of the quasiparticles. This would elucidate the validity of the Fröhlich Hamiltonian [70] in the weak interaction regime and the study of the role of many-body correlations in the strong interaction regime, going be-

yond the single polaron physics very recently observed in ultracold gases [71, 72]. The newly developed theory of angulon and pendulon quasiparticles could be generalized to include impurity interactions, and could then be realized in the present system [73, 74]. On the other hand, the extension of this proposal to two dimensional quantum gases may help study the quantum phase transition between the superfluid and supersolid and from supersolid to the crystal phase [11], which has been never experimentally achieved in ultracold gases. The formation of crystal structures like those found in magnetic atoms or predicted for polar molecules could be observed as well [25, 28]. These future studies, especially when the dynamics of the system are considered, depend sensitively on the relationship between the molecular lifetimes and the relevant timescales for many-body physics. The already brief molecular lifetimes of several tens of microseconds may be reduced by interactions. The stability of the system to decay from molecule-molecule collisions or mechanisms such as Penning ionization can be studied using the anisotropic interactions, since these can either be attractive, leading to collapse, or possess a strong repulsive barrier, stabilizing the condensate.

This work is supported in part by the National Science Foundation under Grant No. NSF PHY-1607180 and Grant No. NSF PHY11-25915. M.T. Eiles and C.H. Greene are happy to acknowledge helpful discussions with G. Groenenboom.

---

lar molecules in pendular states," *ChemPhysChem* **17**, 1 (2016).

- [9] J. L. Bohn, M. Cavagnero, and C. Ticknor, "Quasi-universal dipolar scattering in cold and ultracold gases," *New J. Phys.* **11**, 055039 (2009).
- [10] Y. Wang, J. P. D'Incao, and C. H. Greene, "Universal three-body physics for Fermionic dipoles," *Phys. Rev. Lett.* **107**, 233201 (2011).
- [11] M. A. Baranov, M. Dalmonte, G. Pupillo, and P. Zoller, "Condensed matter theory for dipolar quantum gases," *Chem. Rev.* **112**, 5012 (2012).
- [12] I. Danshita and C. A. R. Sá de Melo, "Supersolid phases of dipolar bosons in optical lattices," *Phys. Rev. Lett.* **103**, 225301 (2009).
- [13] L. Santos, G. V. Shlyapnikov, and M. Lewenstein, "Roton-maxon spectrum and stability of trapped dipolar Bose-Einstein condensates," *Phys. Rev. Lett.* **90**, 250403 (2003).
- [14] T. Lahaye, C. Menotti, L. Santos, M. Lewenstein, and T. Pfau, "The physics of dipolar bosonic quantum gases," *Rep. Prog. Phys.* **72**, 126401 (2009).
- [15] T. Lahaye, J. Metz, B. Fröhlich, T. Koch, M. Meister, A. Griesmaier, T. Pfau, H. Saito, Y. Kawaguchi, and M. Ueda, "d-wave collapse and explosion of a dipolar Bose-Einstein condensate," *Phys. Rev. Lett.* **101**, 080401 (2008).
- [16] S. Ronen, D. C. E. Bortolotti, and J. L. Bohn, "Radial and angular rotons in trapped dipolar gases," *Phys. Rev. Lett.* **98**, 030406 (2007).
- [17] I. Tikhonenkov, B. A. Malomed, and A. Vardi, "Anisotropic solitons in dipolar Bose-Einstein condensates," *Phys. Rev. Lett.* **100**, 090406 (2008).
- [18] W. Lechner and P. Zoller, "From classical to quantum glasses with ultracold polar molecules," *Phys. Rev. Lett.* **111**, 185306 (2013).
- [19] B. Gadway and B. Yan, "Strongly interacting ultracold polar molecules," *J. Phys. B* **49**, 152002 (2016).
- [20] F. Cinti, P. Jain, M. Boninsegni, A. Michel, P. Zoller, and G. Pupillo, "Supersolid droplet crystal in a dipole-blockade gas," *Phys. Rev. Lett.* **105**, 135301 (2010).
- [21] K.-K. Ni, S. Ospelkaus, M. H. G. de Miranda, A. Pe'er, B. Neyenhuis, J. J. Zirbel, S. Kotochigova, P. S. Julienne, D. S. Jin, and J. Ye, "A high phase-space density gas of polar molecules," *Science* **322**, 231 (2008).
- [22] J. W. Park, S. A. Will, and M. W. Zwierlein, "Ultracold dipolar gas of fermionic  $^{23}\text{Na}^{40}\text{K}$  molecules in their absolute ground state," *Phys. Rev. Lett.* **114**, 205302 (2015).
- [23] M. Guo, B. Zhu, B. Lu, X. Ye, F. Wang, R. Vexiau, N. Bouloufa-Maafa, G. Quéméner, O. Dulieu, and D. Wang, "Creation of an ultracold gas of ground-state dipolar  $^{23}\text{Na}^{87}\text{Rb}$ ," *Phys. Rev. Lett.* **116**, 205303 (2016).
- [24] T. Takekoshi, L. Reichsöllner, A. Schindewolf, J. M. Hutson, C. R. LeSueur, O. Dulieu, F. Ferlaino, R. Grimm, and H.-C. Nägerl, "Ultracold dense samples of dipolar RbCs molecules in the rovibratioanl and hyperfine ground state," *Phys. Rev. Lett.* **113**, 205301 (2014).
- [25] H. Kadau, M. Schmitt, M. Wenzel, C. Wink, T. Maier, I. Ferrier-Barbut, and T. Pfau, "Oberving the Rosensweig instability of a quantum ferrofluid," *Nature (London)* **530**, 194 (2016).
- [26] I. Ferrier-Barbut, H. Kadau, M. Schmitt, M. Wenzel, and T. Pfau, "Obervation of quantum droplets in a strongly dipolar gas," *Phys. Rev. Lett.* **116**, 215301 (2016).

[27] M. Lu, N. Q. Burdick, S.-H. Youn, and B. L. Lev, "Strongly dipolar Bose-Einstein condensate of dysprosium," *Phys. Rev. Lett.* **107**, 190401 (2011).

[28] T. Lahaye, T. Koch, B. Fröhlich, M. Fattori, J. Metz, A. Griesmaier, S. Giovanazzi, and T. Pfau, "Strong dipolar effects in a quantum ferrofluid," *Nature (London)* **448**, 672 (2007).

[29] T. J. Carroll, K. Claringbould, A. Goodsell, M. J. Lim, and M. W. Noel, "Angular dependence of the dipole-dipole interaction in a nearly one-dimensional sample of Rydberg atoms," *Phys. Rev. Lett.* **93**, 153001 (2004).

[30] S. Ravets, H. Labuhn, D. Barredo, T. Lahaye, and A. Browaeys, "Measurement of the angular dependence of the dipole-dipole interaction between two individual Rydberg atoms at a Förster resonance," *Phys. Rev. A* **92**, 020701 (2015).

[31] G. Pupillo, A. Micheli, M. Boninsegni, I. Lesanovsky, and P. Zoller, "Strongly correlated gases of Rydberg-dressed atoms: quantum and classical dynamics," *Phys. Rev. Lett.* **104**, 223002 (2010).

[32] J. Deiglmayr, M. Aymar, R. Wester, M. Widemüller, and O. Dulieu, "Calculations of static dipole polarizabilities of alkali dimers: prospects for alignment of ultracold molecules," *J. Chem. Phys.* **129**, 064309 (2008).

[33] H. P. Büchler, E. Demler, M. Lukin, A. Micheli, N. Prokof'ev, G. Pupillo, and P. Zoller, "Strongly correlated 2D quantum phases with cold polar molecules: controlling the shape of the interaction potential," *Phys. Rev. Lett.* **98**, 060404 (2007).

[34] S. Giovanazzi, A. Görlitz, and T. Pfau, "Tuning the dipolar interaction in quantum gases," *Phys. Rev. Lett.* **89**, 130401 (2002).

[35] L. F. Gonçalves and L. G. Marcassa, "Control of Rydberg-atom blockade by dc electric-field orientation in a quasi-one-dimensional sample," *Phys. Rev. A* **94**, 043424 (2016).

[36] E. Urban, T. A. Johnson, T. Henage, L. Isenhower, D. D. Yavuz, T. G. Walker, and M. Saffman, "Observation of Rydberg blockade between two atoms," *Nat. Phys.* **5**, 110 (2009).

[37] T. Niederprüm, O. Thomas, T. Eichert, J. Pérez-Ríos, C. H. Greene, and H. Ott, "Observation of pendular butterfly Rydberg molecules," *Nat. Commun.* **7**, 12820 (2016).

[38] C. H. Greene, A. S. Dickinson, and H. R. Sadeghpour, "Creation of polar and nonpolar ultra-long-range Rydberg molecules," *Phys. Rev. Lett.* **85**, 2458 (2000).

[39] E. Fermi, "Sopra lo spostamento per pressione delle righe elevate delle serie spettrali," *Nouvo Cimento* **11**, 157 (1934).

[40] A. Omont, "On the theory of collisions of atoms in rydberg states with neutral particles," *J. Phys. (Paris)* **38**, 1343 (1977).

[41] E. L. Hamilton, C. H. Greene, and H. R. Sadeghpour, "Shape-resonance-induced long-range molecular Rydberg states," *J. Phys. B* **35**, L199 (2002).

[42] A. A. Khuskivadze, M. I. Chibisov, and I. I. Fabrikant, "Adiabatic energy levels and electric dipole moments of Rydberg states of Rb<sub>2</sub> and Cs<sub>2</sub> dimers," *Phys. Rev. A* **66**, 042709 (2002).

[43] M. I. Chibisov, A. A. Khuskivadze, and I. I. Fabrikant, "Energies and dipole moments of long-range molecular Rydberg states," *J. Phys. B* **35**, L193 (2002).

[44] M. T. Eiles and C. H. Greene, "A Hamiltonian for the inclusion of spin effects in long-range Rydberg molecules," (2016).

[45] D.A. Anderson, S. A. Miller, and G. Raithel, "Angular-momentum couplings in long-range Rb<sub>2</sub> Rydberg molecules," *Phys. Rev. A* **90**, 062518 (2014).

[46] S. Markson, S. T. Rittenhouse, R. Schmidt, J. P. Shaffer, and H. R. Sadeghpour, "Theory of ultralong-range Rydberg molecule formation incorporating spin-dependent relativistic effects: Cs(6s)-Cs(np) as case study," *ChemPhysChem* **10**, 1002 (2016).

[47] We work in Hund's case b.

[48] J. M. Rost, J. C. Griffin, B. Friedrich, and D. R. Herschbach, "Pendular states and spectra of oriented linear molecules," *Phys. Rev. Lett.* **68**, 1299 (1992).

[49] B. Friedrich and D. R. Herschbach, "Spatial orientation of molecules in strong electric fields and evidence for pendular states," *Nature (London)* **353**, 412 (1991).

[50] M. Viteau, M. G. Bason, J. Radogostowicz, N. Malossi, D. Ciampini, O. Morsch, and E. Arimondo, "Rydberg excitations in Bose-Einstein condensates in quasi-one-dimensional potentials and optical lattices," *Phys. Rev. Lett.* **107**, 060402 (2011).

[51] H. Margenau, "Van der Waals forces," *Rev. Mod. Phys.* **11**, 1 (1939).

[52] A. Stone, *The theory of intermolecular forces*, 2nd ed. (Oxford University Press, 2013).

[53] G. C. Groenenboom, X. Chu, and R. V. Krems, "Electronic anisotropy between open shell atoms in first and second order perturbation theory," *J. Chem. Phys.* **126**, 204306 (2006).

[54] B. Bussery-Honvault, F. Dayou, and A. Zanchet, "Long-range multipolar potentials of the 18 spin-orbit states arising from the C(<sup>3</sup>P)+OH(<sup>2</sup>Π) interaction," *J. Chem. Phys.* **129**, 234302 (2008).

[55] M. R. Flannery, D. Vrinceanu, and V. N. Ostrovsky, "Long-range interaction between polar Rydberg atoms," *J. Phys. B. At. Mol. Opt.* **38**, S279 (2005).

[56] Ad van der Avoird, Paul E. S. Wormer, Fred Mulder, and Rut M. Berns, "Ab initio studies of the interactions in Van der Waals molecules," in *Van der Waals Systems* (Springer Berlin Heidelberg, Berlin, Heidelberg, 1980) pp. 1–51.

[57] R. J. Le Roy, "Long-range potential coefficients from RKR turning points: C<sub>6</sub> and C<sub>8</sub> for B(<sup>3</sup>Π<sub>Ou</sub><sup>+</sup>)-State Cl<sub>2</sub>, Br<sub>2</sub>, and I<sub>2</sub>," *Can. J. Phys.* **52**, 246 (1974).

[58] M. Peter and M. Strandberg, "High-field stark effect in linear rotors," *J. Chem. Phys.* **26**, 1657 (1957).

[59] J. Bulthuis, J. van Leuken, F. van Amerom, and S. Stottle, "Brute force orientation and the two-dimensional oscillator," *Chem. Phys. Lett.* **222**, 378 (1994).

[60]  $\xi = (8\omega)^{1/4} \tan(\theta/2)$ , and terms higher than  $(1/\omega)$  are dropped. The wave function is  $\Psi_{\tilde{N}M_N}(\xi, \phi) = \sqrt{\frac{2\tilde{N}!}{\Gamma(\tilde{N}+m+1)}} (-1)^m \xi^m e^{-\xi^2/2} L_{\tilde{N}}^m(\xi^2) \frac{e^{im\phi}}{\sqrt{2\pi}}$ , where  $L_a^b(x)$  is an associated Laguerre polynomial and  $m = |M_N|$ .

[61] We find:  $C_{6i}^a/C_{6d}^a = 2 + 5/(2\omega) - 2\sqrt{2/\omega}$  and  $C_{6d}^c/C_{6d}^a = 9 + 9\sqrt{2/\omega^3} - 9/(2\omega) - 225/8\omega^2$ .

[62]  $C_{6i}^b/C_{6d}^a \sim 36\sqrt{2\omega}$ , which is  $\sim 1000$  for the range of  $\omega$  considered here.

[63] For  $n = (20, 22, \dots, 38, 40)$  the values of  $\Theta_{M,n}$  were (57.3, 57.3, 57.3, 57.2, 57.1, 57.2, 57.1, 57.0, 56.9, 56.8, 56.7) degrees. The break in monotonicity is due to the shift in well position for  $n = 30$ .

[64] T. Manthey, T. Niederprüm, O. Thomas, and H. Ott, “Dynamically probing ultracold lattice gases via rydberg molecules,” *New. J. Phys.* **17**, 103024 (2015).

[65] J. Tallant, S. T. Rittenhouse, D. Booth, H. R. Sadeghpour, and J. P. Shaffer, “Observation of blueshifted ultralong-range  $Cs_2$  Rydberg molecules,” *Phys. Rev. Lett.* **109**, 173202 (2012).

[66] D. Booth, S. T. Rittenhouse, J. Yang, H. R. Sadeghpour, and J. P. Shaffer, “Production of trilobite Rydberg molecule dimers with kilo-Debye permanent electric dipole moments,” *Science* **348**, 99–102 (2015).

[67] M. T. Eiles and C. H. Greene, “Ultracold long-range Rydberg molecules with complex multichannel spectra,” *Phys. Rev. Lett.* **115**, 193201 (2015).

[68] A. T. Krupp, A. Gaj, J. B. Balewski, P. Ilzhöfer, S. Hofferberth, R. Löw, T. Pfau, M. Kurz, and P. Schmelcher, “Alignment of  $D$ -state Rydberg molecules,” *Phys. Rev. Lett.* **112**, 143008 (2014).

[69] W. Li, T. Pohl, J. M. Rost, Seth T. Rittenhouse, H. R. Sadeghpour, J. Nipper, B. Butscher, J. B. Balewski, V. Bendkowsky, R. Löw, and T. Pfau, “A homonuclear molecule with a permanent electric dipole moment,” *Science* **334**, 1110–1114 (2011).

[70] H. Fröhlich, H. Pelzer, and S. Zienau, “Properties of slow electrons in polar materials,” *Philosophical Magazine* **31**, 221 (1950).

[71] N.B. Jørgensen, L. Wacker, K.T. Skalmstang, M. M. Parish, J. Levinsen, R. S. Christensen, G. M. Bruun, and J. J. Arlt, “Observation of attractive and repulsive polarons in a Bose-Einstein condensate,” *Phys. Rev. Lett.* **117**, 055302 (2016).

[72] M.G. Hu, M. J. Van de Graaff, D. Kedar, J. P. Corson, E. A. Cornell, and D. S. Jin, “Bose polarons in the strongly interacting regime,” *Phys. Rev. Lett.* **117**, 055301 (2016).

[73] E. S. Redchenko and Mikhail Lemeshko, “Libration of strongly-oriented polar molecules inside a superfluid,” *ChemPhysChem* **17**, 3649–3654 (2016).

[74] Richard Schmidt and Mikhail Lemeshko, “Rotation of quantum impurities in the presence of a many-body environment,” *Phys. Rev. Lett.* **114**, 203001 (2015).